# Dynamic Analysis of the Non-Linear Behavior of a Composite Sandwich Beam with a Magnetorheological Elastomer Core

N. Chikh, A. Nour, S. Aguib, Imad Tawfiq

# Dynamic Analysis of the Non-Linear Behavior of a Composite Sandwich Beam with a Magnetorheological Elastomer Core

**N. Chikh**[1] **A. Nour**[1⋆] **S. Aguib**[1] **I. Tawfiq**[2]

([1] *Dynamic of Engines and Vibroacoustic Laboratory, M'Hamed Bougara University of Boumerdes, Algeria*)

([2] *Laboratoire QUARTZ(EA*7393*), Supmeca,* 3 *rue de Fernand Hainaut,* 93407 *Saint-Ouen Cedex, France*)

**ABSTRACT** This work deals with the active control of the vibrations of mechanical structures incorporating magnetorheological elastomer. The damping coefficient and shear modulus of the elastomer increase when exposed to a magnetic field. Compared with the vibration control where the elastomer is permanently exposed to a magnetic field, the control of this process through time reduces vibrations more effectively. The experimental study for the vibrations of a sandwich beam filled with an elastomer is conducted, followed by a numerical study using the Abaqus code. The vibration damping is found to be dependent on the loading rate of micro-size ferromagnetic particles in the elastomer.

**KEY WORDS** sandwich beam, magnetorheological elastomer, magnetic field, stiffness, loss factor

**Nomenclature**

| | |
|---|---|
| $E$ | Young's modulus |
| $G$ | Shear modulus |
| $E_i\,(i=b,t)$ | Young's modulus of two skins |
| $\eta$ | Loss factor |
| $G^*$ | Complex shear modulus of elastomer core |
| $G'$ | Elastic modulus of elastomer core |
| $G''$ | Loss modulus of elastomer core |
| $G_c$ | Shear modulus of the elastomer |
| $F_m$ | Excitation magnetic force |
| $B_r$ | Remanent induction |
| $\nabla H$ | Gradient of the magnetic field |
| $V$ | Volume of the magnet |
| $F$ | Total force subjected by the beam |
| $y$ | Total deformation in inflection of the beam |
| $y_i\,(i=b,t)$ | Deformation in inflection of two skins |
| $y_c$ | Deformation in inflection of the elastomer core |
| $K_g$, $K_s$ | Coefficients of the beam |
| $L$ | Length of the beam |
| $b$ | Width of the beam |
| $h$ | Thickness of the beam |

⋆ Corresponding author. E-mail: aguib2011@yahoo.fr

| | |
|---|---|
| $h_i\,(i=b,t)$ | Thickness of the aluminum skins |
| $h_c$ | Thickness of the elastomer core |
| $D$ | Rigidity of the aluminum skins |
| $I$ | Quadratic moment |
| $\sigma_i\,(i=b,t)$ | Compression or tensile stresses in the aluminum skins |
| $\tau_c$ | Shear stress in the elastomer core |
| $K$ | Structural rigidity of the beam |
| $M$ | Bending moment harp effort |
| $T$ | Shear effort |
| $\nu$ | Poisson's ratio |
| $\rho_i\,(i=b,t,c)$ | Mass density of the top ($t$) and bottom ($b$) skins and the core ($c$), respectively |

# I. Introduction

Magnetorheological elastomers (MRE) are a class of solids that consist of a polymeric matrix with embedded micro or nano-sized ferromagnetic particles. Such composite microstructures are used because of their low elastic constant of a few MPa, which allows high strains. The magnetic interactions of the particles lead to a substantial change in the composite's properties.

The elastic properties of these materials can be tuned by an external magnetic field. Indeed, the interactions between the particles lead to an apparent magnetic stress which changes their elastic behavior. This interaction is dependent on the inner distribution of the particles. In contrast to the usual particles that are randomly dispersed throughout the volume, those subjected to an external magnetic field when the matrix is being cured exhibit an anisotropic distribution. This latter category of MRE is often called the Field Structured Elastomer (FSE). The chain-like, sheet-like, or more complicated structures belong to the FSE type. FSE and MRE exhibit different responses to mechanical solicitations and to magnetic fields.

In recent years, magnetorheological structures have been subject to great attention, due to their moldability, mechanical simplicity, high dynamic range, low power supply, high capacity for damping vibrations, and robustness. The prediction of MRE behavior is thus an important industrial problem, particularly in advanced sectors such as the space and aerospace industries. The technology used for construction improvement is characterized by increasing the stiffness and damping of mechanical structures.

The analysis of the dynamic behavior of mechanical and magnetorheological elastomers has been the subject for several studies[1–5]. The analytical development and numerical simulation of the effect of a magnetic field applied perpendicularly to a magnetorheological sandwich beam were performed[6,7]. These studies showed the dependence of the beam's dynamic properties, especially its shear modulus, on the variation of the magnetic field. Nayak et al.[8,9] studied the stability of a simply supported magnetorheological sandwich beam subjected to a dynamic axial force using the Galerkin method. This study demonstrated that the stability of the beam was significantly enhanced by the application of the magnetic field. In the succeeding study, Nayak et al. used the Finite Element Method (FEM) to validate the previous one. Dwivedy et al.[10] presented the regions of instability of a sandwich beam subjected to a magnetic field applied to a periodic dynamic force. This study showed the advantage of using a magnetorheological elastomer to actively control the vibration of the beam. More recently, studies have been focused on the magnetorheological elastomer beams. Yeh[11] studied the free vibration of magnetorheological elastomer sandwich beams, where the damping and natural frequencies of the plate were calculated using the finite element method. Ying et al.[12] studied the forced vibrations of a magnetorheological elastomer sandwich using a random excitation plate, where the responses of the elastomer were determined using the Galerkin method.

The present work analyzes how magnetic fields change the dynamic property of an MRE embedded viscoelastic core sandwich beam with conductive skins. Aguib et al.[13] studied the dynamic behavior of a magnetorheological elastomer sandwich plate using the Ritz approximation method, the Abaqus finite element software and an experimental method. They determined the forced response, the loss factor of elastic moduli, the rigidity versus the frequency of the plates and the magnetic field.

Comparison of the experimental results versus the numerical ones using the Abaqus finite element software and the Ritz approximation for an appropriate model were made for various plate dimensions

and boundary conditions. Baromiej et al.[14] studied the semi-active control of a sandwich beam partially filled with magnetorheological elastomer. In this work the authors described an analytical model and defined the control problem to which the analytical formula was applied. The numerical solution of the minimization problem resulted in a periodic, perfectly rectangular control function when free vibrations were considered. Such a temporary magnetic field was more efficient than a permanent one. Khimi et al.[15] tested the energy absorption capacity of magnetorheological elastomer and compared it with that of a natural elastomer. The mechanical properties were measured using the dynamic mechanical analysis (DMA) with a frequency ranging from 0.01 to 130 Hz. Sedlacek et al[16] studied the rheological performance of magnetorheological elastomers (MRE) with randomly distributed particles based on the modified magnetic particles and electromagnetic shielding properties.

Although many studies have been reported on the free vibration of sandwich beams with viscoelastic cores, very few have been focused on the free vibration analysis of simply supported MRE embedded viscoelastic sandwich beams[7,9,10]. Similarly, much attention has been given to the parametric instability regions of sandwich beams with a viscoelastic core and MRE patches[10]. The work presented here assesses the potential of MRE developed for vibration damping. MRE beams have been widely used in civil and mechanical engineering because of its ability to absorb undesirable electromagnetic signals and wave pollution. The objective of the MRE beam design, as shown in Fig.1, is to obtain a material of the minimum thickness and the lowest possible reflectance within the widest possible operating bandwidth. The dynamic properties of isotropic and anisotropic elastomers, shown in Fig.2, were determined experimentally. These MRE properties are exploited in both the experimental and the numerical methods implemented.

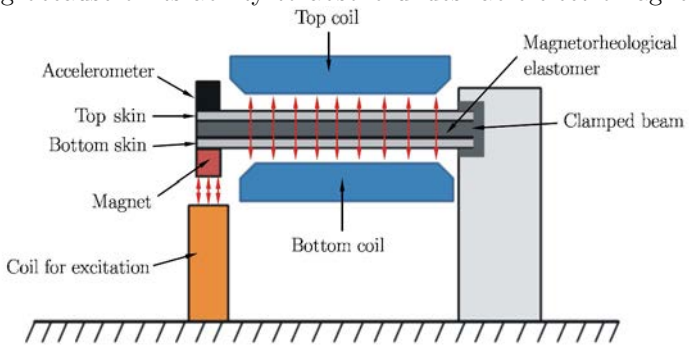


Fig. 1 Sandwich beam subjected to a magnetic field.

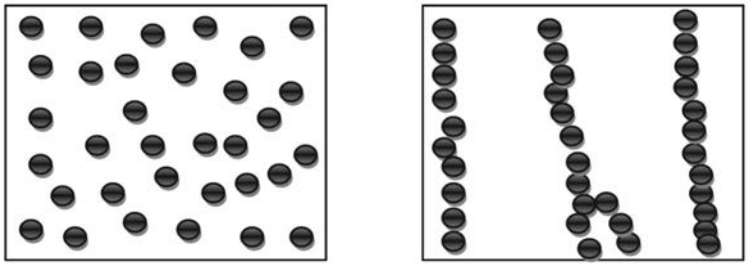

(a) Isotropic MRE (b) Anisotropic MRE

Fig. 2. Magnetorheological elastomer structure.

## II. Mathematical Formulation

In this section, different formulas used in the experiments to determine different properties of viscoelastic materials are presented. The behavior of viscoelastic material is intermediate between those of an ideal elastic solid symbolized by elastic modulus $E$ (or $G$) and a Newtonian viscous liquid damper symbolized by viscosity $\eta$.

To reflect the duality between viscosity and elasticity, when a material is subjected to dynamic shear load, the complex modulus $G^*$ is frequently used[11,17]:

$$G^* = G' + \mathrm{i}G'' = G_c\,(1 + \mathrm{i}\eta) \tag{1}$$

where $G'$, the real part of $G^*$, is called the storage modulus which characterizes the stiffness of the viscoelastic material; and $G''$, the imaginary part, is called the dissipation module, which characterizes the viscous behavior. The loss factor or damping factor can be written as[18]

$$\tan(\delta) = \frac{G''}{G'} = \eta \tag{2}$$

The excitation force of the beam is given by[13,19,20]

$$F_m = B_r \times \nabla H \times V \tag{3}$$

where $B_r$ is the remanent induction of the magnet (0.7 T in our experiments), $\nabla H$ is the field gradient (measured as 1200 A/m per mm at a distance of 2 cm from the core and at a current of 0.7 A), $V$ is the volume of the magnet ($10^{-6}$ m$^3$), and $F_m = 2.59$ N. The overall load supported by the beam is given as a function of the stiffnesses of the two aluminum skins and the magnetorheological elastomer, as well as the deformations of the two aluminum skins $y_i\,(i = t, b)$ and the elastomer $y_c$.

In the case of a clamped-free beam, as shown in Fig.1, the relationship of the overall strength is given as follows[21,22]:

The bending deformation $y$ is equal to:

$$y = y_{t,b} + y_c \tag{4}$$

$y_i\,(i = t, b)$ is the term associated with the bending of the rigid aluminum skins:

$$y_{t,b} = \frac{K_g \times B_r \times \nabla H \times V \times L^3}{EI} \tag{5}$$

$$D = EI \tag{6}$$

with:

$$E = E_i \left(1 - \frac{h_c^3}{h^3}\right)$$

The bending $y_i\,(i = t, b)$, proportional to the cube of length, is usually dominant, especially for a large span compared to the thickness of the sandwich. In a configuration of a given strength and scope, we seek to reduce the sag and increase the rigidity $D = EI$. To this end we can either increase the elastic modulus $E$ of the two skins by changing the material, or increase the inertia by increasing the thickness. This is the simplest conventional solution which follows the sandwich structure; In this paper a recent method is applied to improve the stiffness and the loss factor of the sandwich structure by using a magnetorheological elastomer. The term $y_c$ is related to the elastomeric shear deformation:

$$y_c = \frac{K_s \times B_r \times \nabla H \times V \times L}{G_c \times b \times (h_c + h_i)} \tag{7}$$

The shear deflection $y_c$, proportional to the length, is generally low unless the supports are close and the shear is high. The structural rigidity of the beam is given by:

$$K = \frac{EI}{L^3} + (h_i + h_c) \times G_c \tag{8}$$

The relationship of the overall strength is given as follows[22]:

$$F = \left[\frac{EI}{L^3} + (h_i + h_c) \times G_c\right] \times \left[\frac{K_g \times B_r \times \nabla H \times V \times L^3}{EI} + \frac{K_s \times B_r \times \nabla H \times V \times L}{G_c \times b \times (h_c + h_i)}\right] \tag{9}$$

The stresses in tension or compression in the skin are given by the following formula:

$$\sigma_i = 2\frac{M(x)}{Lh_i(h_i + h_c)} = 2\frac{B_r \times \nabla H \times V \times (L - x)}{Lh_i\,(h_i + h_c)} \tag{10}$$

The shear stress in the elastomer is given by the formula:

$$\tau_c = \frac{T}{L(h_i + h_c)} = \frac{B_r \times \nabla H \times V}{L\,(h_i + h_c)} \tag{11}$$

where $M(x)$ and $T$ are the bending moment and shear force, respectively.

In the case of a free clamped beam subjected to a concentrated force on the free edge, the values for the constants $K_g$ and $K_s$ shown in expressions (5) and (8) are given as follows : $K_g = \frac{1}{3}$, $K_s = 1$.

## III. Experimental Technique

In this study, a magnetorheological elastomer containing iron particles at the volume fraction of 40% was prepared and characterized by a dynamic shear test. The technique of the constant frequency was applied to characterize the elastic and vibration damping properties of the MRE by using the DMA + 450 MetraviB viscoanalyzer.

The spring elements consisting of aligned and isotropic MRE with 40% iron particles were studied both without any magnetic field and with increasing field strength under dynamic shear loading. The dynamic stiffness and the loss factor values were calculated from the measured force-displacement loops. For shear testing in the magnetic field, a special coil device was designed so that the shear load and the magnetic field direction could be applied parallel to the chain direction aligned in the MRE. The effect of MR on the testing frequency and strain amplitude was studied to explore the possible use of MRE in low-frequency structural applications with varying loads and strains. In addition, the static stiffness of the aligned MRE with 40% volume of Fe was measured as a function of the magnetic field strength.

### 3.1. Development of the magnetorheological elastomer

The elastomer was prepared as per the following steps:

1 - Silicone oil and RTV141A polymer was mixed in a vessel manually for 10 minutes to obtain a well-homogenized elastomer gel.

2 - An amount of the gel obtained in the previous step was mixed for 15 minutes with a quantity of iron particles until homogeneous. This resulted in an elastomer comprising 40% volume of iron particles.

3 - To remove the air bubbles infiltrated during mixing, the mixture was degassed for 10 minutes using a vacuum pump. The elastomer obtained was stored hermetically at low temperature.

The ingredients of the magnetorheological elastomer specimen in rectangular shape, 35 mm long, 20 cm wide and 2 mm thick, comprising 40% volume of iron particles are shown in Fig.3. The constituent elements of the magnetorheological elastomer are given in Table 1.

Fig. 3. Ingredients of the magnetorheological elastomer.

Table 1. **Constituents of the magnetorheological elastomer**

| Beam comprising 40% ferromagnetic particles | | | | |
|---|---|---|---|---|
| Cross linking time in hours | $m_{\text{silicone\_oil}}$ (g) | $m_{\text{RTV(A)}}$ (g) | $m_{\text{Fe}}$ (g) | $m_{\text{RTV(B)}}$ (g) |
| 24 | 2.62 | 2.60 | 18.90 | 0.26 |

The viscoelastic properties of the synthesized MRE sample were characterized by the DMA + 450 MetraviB viscoanalyzer shown in Fig.4.

The storage and loss moduli, $G'$ and $G''$, were measured over the frequency range of 0.01-100 Hz, both in the presence and in the absence of a magnetic field. The results of the measurements are summarized in Table 2.

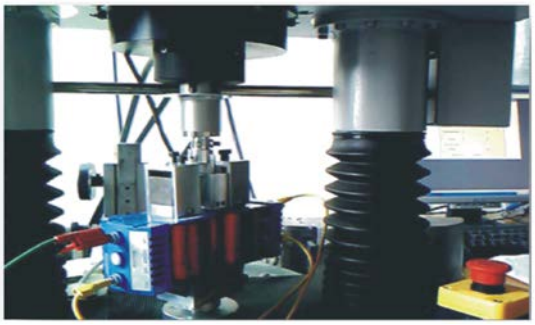

Fig. 4. DMA + 450 MetraviB viscoanalyzer.

Table 2. **Experimental shear moduli $G'$ and $G''$**

| $I = 0$ A | | $I = 0.5$ A | | $I = 1.2$ A | | $I = 2$ A | |
|---|---|---|---|---|---|---|---|
| $G'$ (MPa) | $G''$ (MPa) | $G'$ (MPa) | $G''$ (MPa) | $G'$ (MPa) | $G''$ (MPa) | $G'$ (MPa) | $G''$ (MPa) |
| 1.8328 | 0.3236 | 2.1461 | 0.7036 | 3.1527 | 1.0334 | 2.9660 | 0.7248 |
| 1.2847 | 0.3148 | 1.5403 | 0.5410 | 2.1824 | 0.7340 | 2.5806 | 0.6335 |
| 1.01643 | 0.2495 | 1.2133 | 0.4019 | 1.6262 | 0.5323 | 2.3134 | 0.5763 |
| 0.8186 | 0.2200 | 0.8716 | 0.2979 | 1.1262 | 0.3482 | 1.7035 | 0.4636 |
| 0.6805 | 0.1895 | 0.7658 | 0.2770 | 0.8908 | 0.2947 | 1.3160 | 0.3595 |
| 0.6197 | 0.1521 | 0.7143 | 0.2317 | 0.7546 | 0.3206 | 1.1240 | 0.3136 |

### 3.2. Elaboration of the magnetorheological sandwich beam

After evaluating the influence of the magnetic field on the elastomer comprising 40% volume of iron particles, and given the lack of literature on magnetorheological sandwich beams, we found it particularly interesting to study the influence of the magnetic field on the vibrational behavior of these beams. The objective was to develop a sandwich beam containing an MRE with micro sized iron particles at a volume fraction of 40%. The particles had to be aligned before crosslinking under the effect of a constant magnetic field to obtain a structure with viscoelastic properties that can be tuned by a magnetic field applied externally.

*3.2.1. Implementation of the preparation*

A rubber mold of rectangular form, 15 cm in length, 3 cm in width and 2 mm in thickness, was bonded to the lower aluminum skin of the beam (Fig.5(a)). Dough of the elastomer was injected into the mold (Fig.5(b)). The upper skin on the elastomer was bonded to prevent separation (Fig.5(c)).

The beam obtained was subjected to a perpendicular constant magnetic field (0.14 T) so that the ferromagnetic particles could be aligned during the crosslinking of the elastomer (Fig.6).

The mechanical and geometrical properties of the beam are given in Tables 3 and 4.

Table 3. **Mechanical and electrical properties of the beam**

| Material properties | $\rho$ (kg/m$^3$) | $E$ (MPa) | $\nu$ | $\mu_{ej}$ (Hm$^{-1}$) |
|---|---|---|---|---|
| Aluminum skins | 2800 | 72000 | 0.33 | $1.2566650\times10^{-6}$ |
| Elastomer | 1100 | 1.7 | 0.45 | |

Table 4. **Parameters of the sandwich beam**

| Geometrical characteristics of the top ($t$) and bottom ($b$) skins | | | |
|---|---|---|---|
| $a$ (mm) | $L$ (mm) | $d_t$ (mm) | $d_b$ (mm) |
| 30 | 150 | 1 | 1 |
| **Geometrical characteristics of the elastomer** | | | |
| $a$ (mm) | $L$ (mm) | $d_c$ (mm) | |
| 30 | 150 | 2 | |


(a) Aluminum top and bottom skins

(b) Injected elastomer into the mold


(c) MRE beam

Fig. 5. Steps in fabricating the MRE beam.

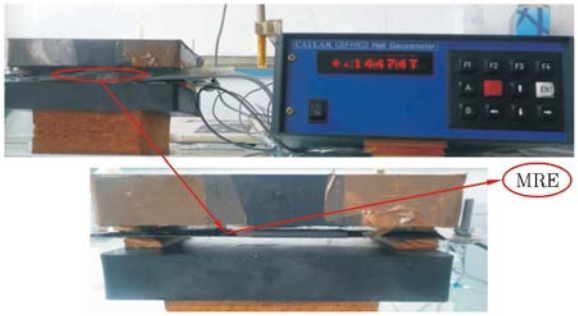


Fig. 6. Device for crosslinking the elastomer loaded with 40% volume of iron particles.

*3.2.2. Experimental device and determination of the vibrational response*

• **Experimental device**

As shown in Fig.7, the second experiment was performed to determine the vibrational response of the beam by applying a constant magnetic field of different intensities by means of the electromagnet 6 on beam 3. The magnet was glued on the free side of the beam excited by the magnetic force generated from the excitation coil 4 powered by the alternating current of a frequency ranging between 0 and 160 Hz. This created a vibratory motion of the beam; The intensity of the current was measured by the current loop transducer 5. The amplitude of vibration was varied using the frequency generator 8 which powered the excitation coil 4 with an alternating current. The vibrational response of the beam was measured by the accelerometer 2 connected to the digital oscilloscope 7.

This device consisted of:

1. a high current power supply for the electromagnet 6; 2. an accelerometer; 3. an MRE sandwich; 4. an excitation coil generating electromagnetic force; 5. a current loop transducer; 6. an electromagnet generating the magnetic field applied to the MRE; 7. a digital oscilloscope; 8. a frequency generator; 9 and 10. laptop computers to drive the power supply 1 and to acquire the data from the accelerometer 2; and 11. a magnet glued to the free end of the beam.

• **Experimental results and discussion**

The amplitude response corresponding to the first mode of vibration of the sandwich beam with a magnetorheological elastomer core at 27°C and a harmonic load is shown in Fig.8 for different values of magnetic field intensity. It is noted that when the frequency is far from the resonance frequency, the amplitude responses obtained are very low and the amplitude corresponding to the resonance frequency

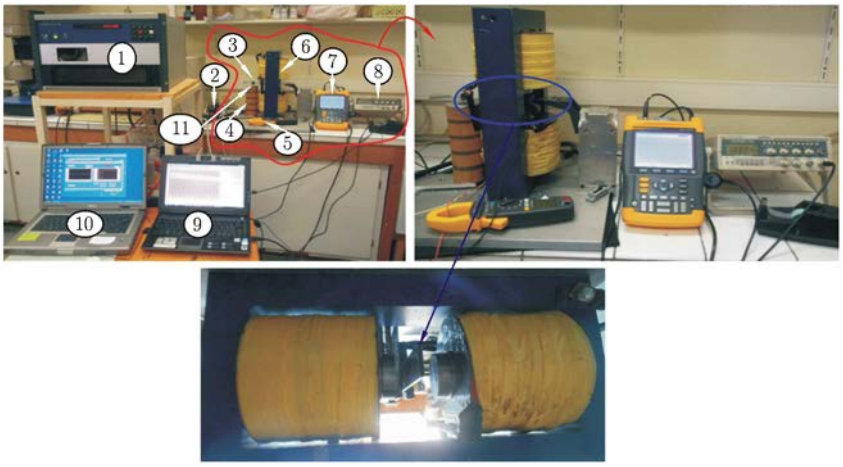


Fig. 7. Experimental device for determining the forced vibrational response of the beam.

of 9.11 Hz decreases as the intensity of the magnetic field generated by the electromagnet 6 increases (Fig.7). This observation can be clearly seen in Fig.9, where the vibration amplitude at the resonance frequency is shown as a function of the induction of the magnetic field applied to the MRE core of the sandwich beam.

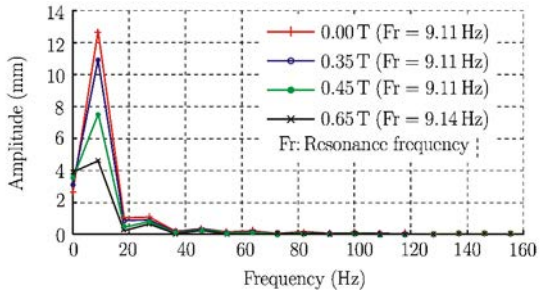


Fig. 8. Variation of the amplitude versus excitation frequency in the magnetic field.

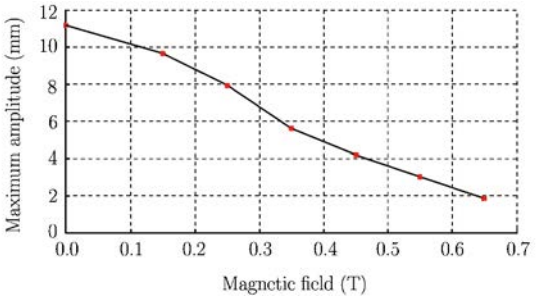


Fig. 9. Variation of the maximum vibration amplitude versus the magnetic field.

Figure 10 shows the vibration waveforms of the sandwich beam excited with an external force of 2.59 N and a frequency of 9.11 Hz at different magnetic fields applied to the MRE core. As inferred from this figure, the magnetorheological elastomer provides better damping properties when the magnetic field intensity increases. The aligned particle structure of the MRE core has a significant influence on the viscoelastic properties of the composite material. Either the stiffness or the damping properties of MRE can be increased by applying a magnetic field by optimizing the content of particles and their alignment.

Figure 11 shows that when the intensity of the magnetic field increases, the overall force supported by the beam decreases, which means that the resistant force created by the magnetic field generated by coil 6 becomes greater than the excitation force created by the magnetic field generated by coil 4 where the beam is deformed less and reaches its minimum value.

Figure 12 shows the variation of tensile stresses in the aluminum skins and the shear stresses in the magnetorheological elastomer. Analysis of this figure shows that the values of the skin tensile stresses change considerably and decrease as the intensity of the magnetic field increases; The curve of the corresponding shear stress of the magnetorheological elastomer versus the increase in the magnetic field is quite flat. This infers that the technique of applying a magnetic field provides the optimal elastomer damping properties.

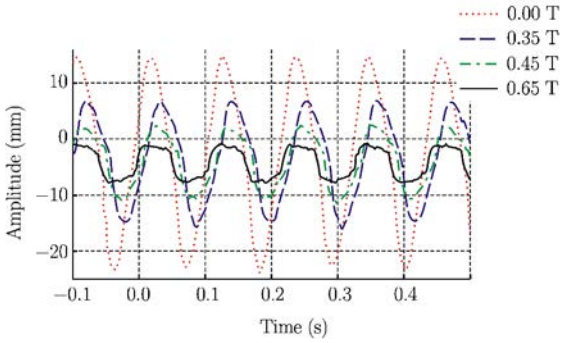


Fig. 10. Variation of the vibration amplitude versus time, the excitation force amplitude is 2.59 N and the excitation frequency is 9.11 Hz.

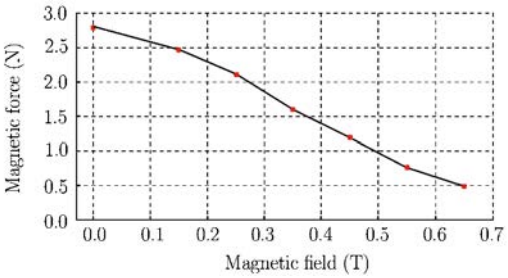


Fig. 11. Variation of the overall force as a function of the magnetic field intensity.

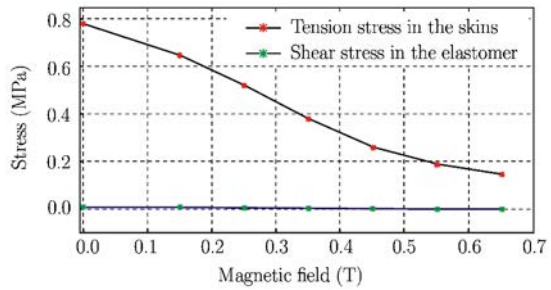


Fig. 12. Influence of the magnetic field intensity on the stresses of the beam.

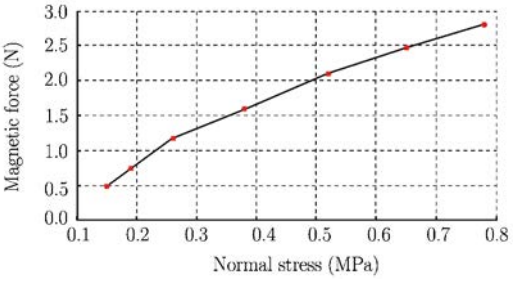


Fig. 13. Variation of magnetic force as a function of stress of the beam.

Figure 13 shows that the overall magnetic force increases with the increasing stress. This force continues to vary as a function of the magnetic field intensity in the coil cross-linking in the elastomer. Thus its rheological characteristics change as a function of the intensity of the magnetic field.

Figure 14 shows the dependence of loss factor on the beam frequency. With increasing magnetic field, the electromagnetic force acting on the micro-size ferromagnetic particles increases and creates a pseudo fiber chain. The rigidity of the beam is thus increased. Moreover; the sliding displacement of these particles creates a dissipation of energy, resulting in an increase of the damping. It is the particularity and the advantage over polymer properties (not subject to a magnetic field).

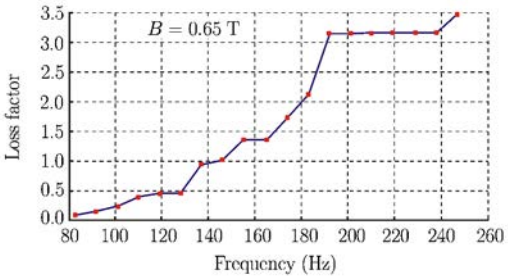


Fig. 14. Loss factor versus the frequency of beam.

## IV. Numerical Modeling

The purpose of this section is to check whether the results obtained from the experiments are reproducible by simulation using the finite element method with the Abaqus calculation code.

As shown in Fig.15(a), the three-layer sandwich structure with a viscoelastic magnetorheological core described previously in the experimental section is viewed in the same spatial configuration relative

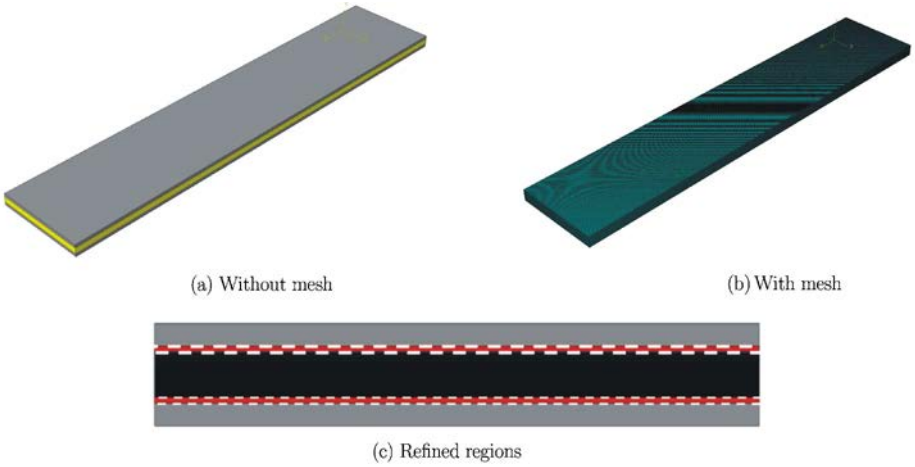


Fig. 15. Geometrical model of the beam.

to the Cartesian coordinate system $(O, x, y, z)$. As before, it is treated as a beam in the present analysis. The notations and conventions already used in §I, §II and §III are used here in the numerical analysis.

In our discretization a linear structured eight-node hexahedral finite element of size $0.2 \times 0.2 \times 0.2$ mm is used, as shown in Fig.15(b). Each node has three degrees of freedom, i.e. a transverse translation in the $y$ direction, a rotation around the $z$ axis and a slip in the interface between the skins and the core. This means that a node at the embedded end needs six essential boundary conditions, including natural and convective. The convective boundary conditions are an essential and natural combination. In Tables 5 and 6 the possible boundary conditions are listed.

Table 5. **Boundary conditions**

| Degree of freedom | Essential | Natural |
|---|---|---|
| Transverse | $w_y$ | Shear force |
| Rotation | $\theta_x$ | Moment |
| Slip | $\Delta_i$ | Normal (anchoring) force |

Table 6. **Boundary conditions in displacement and rotation**

| Case | Condition |
|---|---|
| Clamped ($z = 0$) | $w = 0$ |
| | $\theta_x = 0$ |
| Free ($z = l$) | $\dfrac{\partial^2 w}{\partial y^2} = 0$ |
| | $\dfrac{\partial^3 w}{\partial y^3} = 0$ |

The comparison of the numerical results with those found experimentally shows that the numerical results converge from only 250000 elements for a single skin and 500000 for the core elements in the magnetorheological elastomer. In our case we have specified different sizes of elements within the same mesh. This is the best choice since the stress gradients are not uniform. The stress gradient is observed to be very high at the skin-core interface, as can be seen in Fig.15(c). As the beam has a regular geometry, all the elements are in the same type. This condition allows automatically checking on whether the elements are connected and the element faces are all the same with coinciding edges and nodes. The discretization results are summarized in Table 7.

Table 7. **Discretization of data of the beam**

| Before refinement | | |
|---|---|---|
| Number of elements | Number of nodes | Degree of freedom |
| 2250000 | 2381421 | 7134750 |
| After refinement at interfaces | | |
| 13950000 | 14175125 | 42514050 |

Modeling the viscoelastic behavior of the elastomer is taken into account through a generalized Maxwell model with six branches, since it has been found that considering more branches does not significantly improve the results, regardless of the time scale of the relevant test. The relaxation time is selected such that $\forall i \in [1, 20]$, $\tau_i = 10^{i-12}$ s.

## V. Comparison of Results and Validation

Figures 16 and 17 show the maximum amplitude and stresses found using the experimental and the finite element method based on different magnetic field intensities. As can be seen in Figs.16 and 17, there is a slight difference between the values obtained experimentally and those calculated using the finite element method. The average error between the two methods is about 6.10% in the case of the maximum amplitude (Table 8), and approximately 11.7% in the case of stress in the two aluminum skins and 3.66% for the elastomeric shear (Table 9). It is noted that according to the following tables, there is a relatively significant difference between the experimental results and the results given by Abaqus. This can be explained by the complexity of the model used in Abaqus (viscoelasticity+ dynamic). We note that the complexity of modeling with the Abaqus code leads to difficulties in convergence, which may explain the small difference.

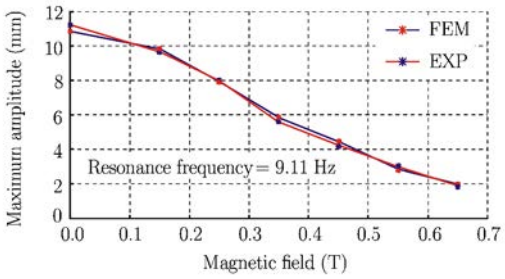


Fig. 16. Comparison of the maximum amplitude versus the magnetic field intensity in the two methods: experimental and FEM.

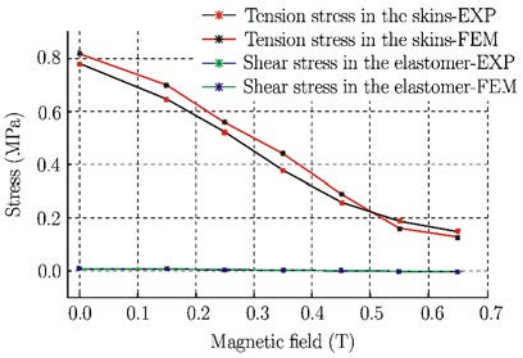


Fig. 17. Comparison of the influence of magnetic field intensity on the stresses of the beam as a function of the experimental and the FEM methods.

Table 8. **Comparison of amplitude values found using the two methods: experimental and FEM**

| Maximum amplitude (mm) | | |
|---|---|---|
| Experimental | FEM | $\Delta$% |
| 10.85 | 11.19 | 03.13 |
| 09.80 | 09.65 | 01.55 |
| 07.92 | 07.96 | 00.50 |
| 05.82 | 05.61 | 03.74 |
| 04.41 | 04.20 | 05.00 |
| 02.84 | 03.00 | 05.63 |
| 01.98 | 01.86 | 06.10 |

Table 9 shows the tensile stress values obtained in the two skins and the shear stress produced in the elastomer core. The comparison of the results obtained from the experiments with those obtained using the finite element method shows a small difference: a maximum difference of 17.31% in the tensile stress and a maximum difference of 11.54% in the shear stress. Despite the technological difficulty in formulating these structures and the mesh refinement at the interfaces of different materials, the experimental and numerical results are very comparable.

Table 9. **Comparison of the tension stress in the skins and shear stress in the elastomer obtained using the two methods: experimental and FEM**

| Tensile stress in the skins (MPa) | | | Shear stress in the elastomer (MPa) | | |
|---|---|---|---|---|---|
| Experimental | FEM | $\Delta\%$ | Experimental | FEM | $\Delta\%$ |
| 0.78 | 0. 82 | 05.13 | $0.85\times10^{-2}$ | $0.94\times10^{-2}$ | 10.59 |
| 0.65 | 0.70 | 07.70 | $0.66\times10^{-2}$ | $0.72\times10^{-2}$ | 09.10 |
| 0.52 | 0.56 | 07.70 | $0.46\times10^{-2}$ | $0.51\times10^{-2}$ | 10.87 |
| 0.38 | 0.44 | 15.80 | $0.26\times10^{-2}$ | $0.29\times10^{-2}$ | 11.54 |
| 0.26 | 0.29 | 11.54 | $0.13\times10^{-2}$ | $0.14\times10^{-2}$ | 07.69 |
| 0.19 | 0.16 | 18.75 | $0.11\times10^{-2}$ | $0.12\times10^{-2}$ | 09.10 |
| 0.15 | 0.13 | 15.40 | $0.10\times10^{-2}$ | $0.11\times10^{-2}$ | 10.00 |

## VI. Discussion and Conclusion

This article was devoted to the experimental and numerical analyses of the vibration response of a magnetorheological elastomer sandwich beam with and without the influence of different magnetic field intensities, when subjected to harmonic excitation by an external force applied on the free end of the beam. The numerical and experimental tests were conducted on a sandwich beam with an elastomer core containing micro-particles of iron at a volume fraction of 40%. The frequency and magnetic field dependent viscoelastic behavior of the magnetorheological elastomer introduces complexity when determining the damping properties of a beam and its vibration response directly and accurately.

The experimental and numerical results lead to the following conclusions:

• Mechanical structures with MRE make it possible to tune deformation and damping values under a homogeneous magnetic field.

• The competition between the increase of magnetic stress and composite stiffness when increasing the concentration of magnetic particles is observed, and the maximum strain is obtained for a filling factor of around 20. The magnetization of such particles plays an important role in the magnetostriction curve of the composite. A direct effect of the external field is recorded: the strain is either positive or negative with respect to the sign of the magnetic field applied, as expected from Lanotte's model based on magnetic torque.

• In the presence of vibrations, the beam is rapidly stabilized under the influence of the magnetic field, even at large amplitudes.

• The incorporation of a layer of elastomer containing iron particles in a magnetic field increases rigidity without losing characteristics due to the viscous damping properties of the elastomer.

• The iron content enhances the mechanical characteristics of the elastomer, particularly its stiffness, by creating an attractive force between the iron particles.

• The stiffness and the loss factor can be adjusted intelligently as a function of any probable solicitation.

• This technique allows reducing or even eliminating the transient structural resonances.

Finally, these new magnetorheological structures (beams or plates) have many potential applications in different industries, especially in construction improvement. To develop a functional composite material with favorable damping properties, it is important to monitor the rheological properties and the magnetorheological effect. Rheological properties depend on the MRE microstructure, which in turn depends on the amount of ferromagnetic particles and their arrangement.

## References


[1] Zhou,Y. and Zhang,Y.L., Optimal design of a shear magnetorheological damper for turning vibration suppression. *Smart Mater. Struct.*, 2013, 22: 0964-1726.

[2] Borbáth,T., Günther,S., Yu Borin,D., Gundermann Th. and Odenbach,S., X$\mu$CT analysis of magnetic field-induced phase transitions in magnetorheological elastomers. *Smart Mater. Struct.*, 2012, 21: 0964-1726.

[3] Sedlačík,M., Pavlínek,V., Sáha,P., Švrčinová,P., Filip,P. and Stejskal,J., Rheological properties of magnetorheological suspensions based on core-shell structured polyaniline-coated carbonyl iron particles. *Smart Mater. Struct.*, 2010, 19: 0964-1726.

[4] Li,Y., Li,J., Tian,T. and Li,W., A highly adjustable magnetorheological elastomer base isolator for applications of real-time adaptive control. *Smart Mater. Struct.*, 2013, 22: 0964-1726.

[5] Li,Y., Li,J., Li,W. and Samali,B., Development and characterization of a magnetorheological elastomer based adaptive seismic isolator. *Smart Mater. Struct.*, 2013, 22: 0964-1726.

[6] Zhou,G.Y. and Wang,Q., Use of magnetorheological elastomer in an adaptive sandwich beam with conductive skins. Part I: Magnetoelastic loads in conductive skins. *International Journal of Solids and Structures*, 2006, 43: 5386-5402.

[7] Zhou,G.Y. and Wang,Q., Use of magnetorheological elastomer in an adaptive sandwich beam with conductive skins. Part II: Dynamic properties. *International Journal of Solids and Structures*, 2006, 43: 5403-5420.

[8] Nayak,B., Dwivedy,S.K. and Murthy,K., Multi-frequency excitation of magnetorheological elastomer-based sandwi ch beam with conductive skins. *International Journal of Non-Linear Mechanics*, 2012, 47: 448-460.

[9] Nayak,B., Dwivedy,S.K. and Murthy,K., Dynamic analysis of magnetorheological elastomer-based sandwich beam with conductive skins under various boundary conditions. *Journal of Sound and Vibration*, 2011, 330: 1837-1859.

[10] Dwivedy,S.K., Mahendra,N. and Sahu,K.C., Parametric instability regions of a soft and magnetorheological elastomer cored sandwich beam. *Journal of Sound and Vibration*, 2009, 325: 686-704.

[11] Yeh,J.Y., Vibration analysis of sandwich rectangular plates with magnetorheological elastomer damping treatment. *Smart Mater. Struct.*, 2013, 22: 0964-1726.

[12] Ying,Z.G., Ni,Y.Q. and Ye,S.Q., Stochastic micro-vibration suppression of a sandwich plate using a magnetorheological viscoelastomer core. *Journal of Smart Materials and Structures*, 2014, 23: 025019 (11pp).

[13] Aguib,S., Nour,A., Zahloul,H., Bossis,G., Chevalier,Y. and Lançon,P., Dynamic behavior analysis of a magnetorheological elastomer sandwich plate. *International Journal of Mechanical Sciences*, 2014, 87: 118-136.

[14] Dyniewicz,B., Bajkowski,J.M. and Bajer,C.I., Semi-active control of a sandwich beam partially filled with magnetorheological elastomer. *Mechanical Systems and Signal Processing*, 2015, 60-61: 695-705.

[15] Khimi,S.R. and Pickering,K.L., Comparison of dynamic properties of magnetorheological elastomers with existing antivibration rubbers. *Composites Part B*, 2015, 83: 175-183.

[16] Sedlacik,M., Mrlik,M., Babayan,V. and Pavlinek,V., Magnetorheological elastomers with efficient electromagnetic shielding. *Composite Structures*, 2016, 135: 199-204.

[17] Wang,Y. and Inman,D.J., Finite element analysis and experimental study on dynamic properties of a composite beam with viscoelastic damping. *Journal of Sound and Vibration*, 2013, 332: 6177-6191.

[18] Ooi,L.E. and Ripin,Z.M., Dynamic stiffness and loss factor measurement of engine rubber mount by impact test. *Materials and Design*, 2011, 32: 1880-1887.

[19] Vicente,D.J., Bossis,G., Lacis,S. and Guyot,M., Permeability measurements in cobalt ferrite and carbonyl iron powders and suspensions. *Journal of Magnetism and Magnetic Materials*, 2002, 251: 100-108.

[20] Hoffmann,C. and Franzreb,M., A novel repulsive-mode high gradient magnetic separator. *Part I. Design and experimental results, IEEE T Magn*, 2004, 40: 456-461.

[21] Whitney,J.M., Structural Analysis of Laminated Anisotropic Plates. Technomic Publishing Company, ISBN 87762-518-2, 1987.

[22] Berthelot,J.M., Mechanical Behavior of Composite Materials and Structures. 3rd edition, Technical & Documentation, 1999.